Bone 127 (2019) 635–645

Contents lists available at ScienceDirect

Bone

journal homepage: www.elsevier.com/locate/bone

Full Length Article

Are we crying Wolff? 3D printed replicas of trabecular bone structure demonstrate higher stiffness and strength during off-axis loading

Zach Wood[a,1], Lisa Lynn[a,1], Jack T. Nguyen[a], Margaret A. Black[a], Meha Patel[a], Meir M. Barak[a,b,*]

[a] Department of Biology, Winthrop University, Rock Hill, SC 29733, USA
[b] Department of Veterinary Biomedical Sciences, College of Veterinary Medicine, Long Island University, Brookville, NY 11548, USA

ARTICLE INFO

Keywords:
Bone adaptation
Trabecular bone
3D printing
Bone modeling
Stiffness
Strength

ABSTRACT

Roux's principle of bone functional adaptation postulates that bone tissue, and particularly trabecular bone tissue, responds to mechanical stimuli by adjusting (modeling) its architecture accordingly. Hence, it predicts that the new modeled trabecular structure is mechanically improved (stiffer and stronger) in line with the habitual in vivo loading direction. While previous studies found indirect evidence to support this theory, direct support was so far unattainable. This is attributed to the fact that each trabecular bone is unique, and that trabecular bone tissue tends to be damaged during mechanical testing. Consequently, a unique modeled trabecular structure can be mechanically tested only along one direction and a comparison to other directions for that specific structure is impossible. To address this issue, we have 3D printed 10 replicas of a trabecular structure from a sheep talus cropped along the 3 principal axes of the bone and in line with the principal direction of loading (denoted on-axis model). Next, we have rotated the same cropped trabecular structure in increments of 10° up to 90° to the bone principal direction of loading (denoted off-axis models) and printed 10 replicas of each off-axis model. Finally, all on-axis and off-axis 3D printed replicas were loaded in compression until failure and trabecular structure stiffness and strength were calculated. Contrary to our prediction, and conflicting with Roux's principle of bone functional adaptation, we found that a trabecular structure loaded off-axis tended to have higher stiffness and strength values when compared to the same trabecular structure loaded on-axis. These unexpected results may not disprove Roux's principle of bone functional adaptation, but they do imply that trabecular bone adaptation may serve additional purposes than simply optimizing bone structure to one principal loading scenario and this suggests that we still don't fully understand bone modeling in its entirety.

1. Introduction

Almost twenty years ago, Dr. John Currey wrote the following insightful remark regarding Wolff's law: “Wolff [1] stated (to paraphrase him) that boney structures modeled so as to fit them to their function. He wrote a great deal more, of course. The unfortunate thing is that, for many workers, it seems only necessary to show that bone is adapting, invoke Wolff's law, and depart, conscious of a day's work well done. No thought is given as to how the bone models in an adaptive fashion” [1]. Since this statement was written, we have gained much more understanding about how bone structure, and more specifically trabecular bone structure, is adapting its architecture in response to mechanical stimuli. It is now accepted that Wolff's law as Dr. Julius Wolff originally meant it [2] - an exact mathematical response of trabecular architecture to the requirements of maximal performance to minimal weight, is erroneous [3]. The more accurate interpretation of bone modeling is along the lines of Wilhelm Roux's principle of bone functional adaptation - a biological regulatory process governed by mechanical stimuli that leads to bone formation and resorption, and consequently to bone adaptation [4,5].

Nevertheless, Dr. Currey's words are as relevant nowadays as they were then. The complex architecture of trabecular bone tissue, which yield numerous measurable structural parameters (such as bone volume fraction and degree of anisotropy, to name just a few) is hard to interpret, especially since various studies point to different parameters and their combinations as the ones that hold the strongest adaptation “signal” [6–11]. Furthermore, since trabecular bone exists within a cortical bone cortex with which it closely interacts and shares its

* Corresponding author at: Department of Veterinary Biomedical Sciences, College of Veterinary Medicine, Long Island University, 720 Northern Blvd., Brookville, NY 11548, USA.
E-mail address: Meir.Barak@liu.edu (M.M. Barak).
[1] Equal contribution.

https://doi.org/10.1016/j.bone.2019.08.002
Received 28 May 2019; Received in revised form 1 August 2019; Accepted 2 August 2019
Available online 04 August 2019

mechanical function [12–15], studying trabecular bone adaptation separately may give us an incomplete and limited answer. Hence, studying how trabecular bone "models in an adaptive fashion" still poses various difficulties and unknowns. Amongst these unanswered questions, one key problem persists when we try to understand bone adaptation. While we know that trabecular bone responds to mechanical stimuli by modeling, we can't directly quantify how well the new adjusted trabecular structure is adapted to its function. In other words, we don't really know if the new, modeled trabecular structure is mechanically better, worse, or the same compared to the former trabecular structure. And if a mechanical difference does exist, is the outcome of adaptation predominantly affecting the principal physiological direction of loading (making that direction stiffer and stronger compared to other loading directions), or is it affecting the entire structure regardless of the loading direction.

This important problem is derived from two simple facts. The first is that no two trabecular architectures are identical (even when comparing the left and right bones from the same individual). Thus, we can always mechanically test a specific architecture before it was modeled or after the fact, but never both states for the same bone [7,16]. As a result, we can never directly demonstrate the mechanical superiority of a specific modeled trabecular structure over its former state. The second fact is that trabecular bone tissue is a fragile structure and it tends to get damaged and fracture under mechanical testing, hence we generally can test each unique trabecular structure just once [17,18]. Consequently, we have neither a way to repeat the same mechanical test several times to improve the accuracy of our results, nor the ability to mechanically test the same structure in different directions to verify that the modeled structure is truly adapted to its function (i.e. demonstrates superior mechanical properties along the principal physiological direction of loading when compared to other loading directions).

One technique that can be used to address some aspects of this problem is finite element analysis (FEA). FEA is a computer-based method that simulates real world forces and predicts how an object will behave under these conditions. This is accomplished by segmenting the object into numerous discrete elements that are connected by nodes, where each element has its own mathematical equation that describes its mechanical behavior. FEA is widely used to study the mechanical behavior of cortical and trabecular bone tissues under various loading conditions [19–23]. For instance, Bevill and Keaveny [20] examined the ability of linear versus nonlinear FE models to predict bone strength in different anatomical sites and across a range of image resolutions and bone volume fraction (BV/TV). The study results showed that nonlinear FE models yielded better strength predictions, especially when the resolution was below 80 μm (current gold standard resolution of in vivo HR-pQCT is 82 μm), and in samples with lower BV/TV. Nevertheless, the authors acknowledged that HR-pQCT tends to overestimate BV/TV and that this may affect the performance and predictability of these FE models. In addition, there are several further complexities with FEA when it is applied to simulate the mechanical outcome of trabecular modeling. First, to confirm the predictions of FEA, one must always validate it with in vitro mechanical testing [24,25]. Yet this requirement is unachievable when we are trying to simulate the same trabecular structure in different states or to load it from various directions. Since, as mentioned above, every trabecular structure is unique and tends to be damaged under mechanical testing, we cannot attain actual mechanical properties from multiple scenarios and directions of loading for the same trabecular architecture. Second, as simulating the entire trabecular architecture is complicated and requires high computational powers, some studies replace the complex inner 3D trabecular geometry with a solid non-porous volume of lower stiffness elements [23]. Thus, the contributions of trabecular structure and its directionality (anisotropy) are lost. Parr et al. [23] demonstrated that FE models that include trabecular geometry are significantly stiffer than non-porous trabecular FE models and thus they demonstrate lower strains. Furthermore, even when the 3D trabecular architecture is preserved or simulated, FEA studies frequently downscale the resolution of the model, to enable standard computers deal with the millions degrees-of-freedom and solve the huge number of equations. Downscaling and lowering resolution affect how accurate the FE model represents the actual trabecular structure, especially in case of numerous thinner trabeculae. For example, Boyle and Kim [21] used 175 μm voxels to build their simulated human femur, while Christen et al. [22] used downscaled voxels of 26 μm that were able to represent only trabeculae thicker than 80 μm in their mice caudal vertebra model. A further limiting factor of FEA is its comparatively high cost (e.g. Bevill and Keaveny [20] run their FEA on a cluster parallel supercomputer), the relatively steep learning curve of this technique, and the computer coding it frequently requires.

Recent advancements in three-dimensional printing (3DP) enable us to use this relatively new technique as a supplementary method to mechanical testing and computer FEA in studying Roux's principle of bone functional adaptation and the structure-function relationship of trabecular bone [25–32]. Three-dimensional printing is a form of Solid-freeform fabrication (SFF), a technique that facilitates the production of three-dimensional objects from computer aided design (CAD) models. The production takes place by incremental deposition of two-dimensional printing material layers, until a 3D object is created [33,34]. By capturing the 3D image of trabecular bone structure using non-invasive acquisition techniques such as micro computed tomography (micro-CT) and then the use of computer software for segmentation and reconstruction, it is possible to generate 3D CAD models of trabecular bone structure. These models are then exported to a 3D printer that can accurately reproduce the same trabecular architecture as many times as is required. Finally, these replicas can be mechanically tested in various conditions and all the results for an individual trabecular sample could be evaluated and compared. Thus, the use of 3DP enables us to test a unique trabecular structure in multiple loading directions and scenarios. Yet, it is important to understand that when these replicas are mechanically tested, the actual measured stiffness and strength values are less important as they will be significantly different than the bone tissue values. Instead, one should look at the ratio of two or more results from the same trabecular sample to get new insights into which model has superior mechanical properties and in which loading orientations [31].

The goal of this study is to support the prediction of Roux's principle of bone functional adaptation in a direct way for the first time. Roux's principle of bone functional adaptation postulates that bone structure is adapting (modeling) in response to mechanical stimuli by depositing and resorbing bone material and thus it predicts that the new modeled trabecular structure is mechanically superior along the direction of the experienced mechanical stimuli which is transmitted from one cortex to the other. In line with this prediction, and the tension-compression strength asymmetry of bone, discussed by Bevill and Keaveny [20], we hypothesized that a modeled trabecular bone structure will demonstrate higher mechanical stiffness and strength when it is loaded on-axis in comparison to when it is loaded off-axis. Off-axis mechanical behavior refers to the loads that are tilted to the principal material coordinate system of the trabecular structure. To test our hypothesis, we have micro-CT scanned and segmented a trabecular bone sample from a sheep talus. Next, we have cropped the trabecular bone structure in various angles to its principal direction of loading (ranging from 0° to 90° in increments of 10°) to create on- and off-axis models. Each one of the resulting models was replicated 10 times using a 3D printer (ProJet 1200). Finally, all replicas were loaded in compression until failure (Instron 5942) and their mechanical stiffness and strength were measured. If our working hypothesis is supported, then we expect the stiffness and strength values for the on-axis model to be significantly higher compared to the stiffness and strength values for the off-axis models. On the other hand, if our results demonstrate a different trend – either no differences between the models or that the off-axis models

demonstrated higher stiffness and strength values, this will imply that trabecular bone adaptation may serve additional functions other than simply optimizing bone structure to one principal loading scenario. In addition, determining the off-axis mechanical behavior of trabecular bone is beneficial to understanding the etiology of bone fracture and its relationship to off-axis loading such as in the case of falls.

2. Materials and methods

2.1. Bone selection

A talus from a young Dorset sheep (*Ovis aries*) was harvested and cleaned. This sheep took part in a previous study where it trotted on a level treadmill for 15 min/day, 6 days/week for 34 days. Trotting speed was monitored during the experiment to maintain a constant Froude number of 0.35–0.45, which corresponded to 1.35–1.5 m/s on day 32 [7]. The above mechanical stimulus was shown to result in bone modeling, expressed as an increase in bone volume fraction and trabecular number when compared to control sheep that did not trot [7].

The talus was preferred over other bones as it is a short bone that is loaded in sheep almost in perfect compression along its axial axis, between the superior and inferior articular facets (trochlea – articulating with the distal tibia and head - articulating with the proximal navicular respectively). The talus lacks any tendons attachments, it is held in the ankle by the medial and lateral malleolus and constraining ligaments, and thus it experiences loads directly only via its articular facets [35]. In addition, contrary to long bones that have growth plates which yield relatively organized initial trabecular orientation (roughly normal to the growth plate and parallel with the physiological direction of loading), short bones (such as the talus) usually have ossification centers that yield a much less organized initial trabecular structure and thus these structures are less 'biased' toward an initial specific orientation. In the talus, the primary ossification center is situated close to the talar neck [36,37] and a secondary ossification center is very small and is not always present.

2.2. Micro-CT scanning

The talus was micro-CT scanned (Center for Nanoscale Systems, Harvard University) using a Metris X-Tek HMX ST 225 scanner (Nikon Metrology Inc.) at 70 kV and 130 μA with no filter. Scan resolution was 30 μm, which is well below average sheep trabecular thickness (ranges between 50 and 190 μm) as given in previous publications [38–41]. The output raw data was imported into CT-Pro software (Nikon Metrology Inc.) and reconstructed into a 3D volume. Next, the reconstructed 3D volume was imported into a visualization software, VGStudio Max 2.1 (Volume Graphics GmbH, Heidelberg Germany), and was reoriented along the long axis of the bone. The reconstructed scan was then cropped and saved as 16-bit TIFF image stack along the transverse plane. Finally, the image stack was converted into 8-bit TIFF images using ImageJ software version 1.50i, decreasing gray levels from 65,536 to 256 (black pixels equal to "0" and white pixels equal to "255") without affecting spatial resolution.

2.3. Volume cropping and segmentation

The 8-bit TIFF image stack was imported to Amira 6.0 (FEI Visualization Sciences Group Inc.) for segmentation and reconstruction. A cubical volume of interest (VOI) of 7.5 mm^3 (250 $pixels^3$) was cropped from the inferolateral region of the talus, just proximal to the articular facet of the talus head (Fig. 1). After cropping, the image stack was segmented (binarized) to differentiate bone from non-bone pixels. A global gray-scale threshold of 138 was selected by two individual observers to best separate bone from non-bone pixels. Next, to correct possible local inaccuracies, each slide of the original micro CT scan was manually inspected and segmentation was corrected (if necessary) in each of the 3 primary axes (axial, radial, and transverse orientations).

2.4. On-axis model

Using the 7.5 mm^3 VOI, a smaller 4.5 mm^3 VOI (150 $pixels^3$) was cropped from the center of the larger volume and parallel with its planes. This smaller 4.5 mm^3 VOI was denoted 0° as it was not rotated and its surfaces were still oriented along the principal axes of the bone. To verify that the proximal-distal axis of the bone corresponded with the principal trabecular direction we analyzed the 4.5 mm^3 VOI using BoneJ (version 1.4.2) and extracted the corresponding eigenvectors. We found that the principal trabecular direction was almost perfectly aligned with the proximal-distal axis of the bone, tilted by about 6° dorsolaterally.

Once the 4.5 mm^3 VOI was cropped, Amira 6.0 reconstructed a 3D surface model which was then saved in "stl" format and exported to our 3D printer. The 3D printed model was later loaded along its axial orientation to measure the stiffness and strength of the trabecular structure when loaded on-axis, along the physiological direction of loading. These on-axis stiffness and strength values served as a baseline for the off-axis stiffness and strength values.

2.5. Off-axis models

To load the same trabecular structure in directions rotated to the axial orientation, off-axis VOIs were created from within the same original 7.5 mm^3 VOI with increasing rotations to the on-axis 0° 4.5 mm^3 VOI. The on-axis 0° VOI was rotated along the cube center of rotation in increments of 10°, once along the coronal plane (to generate models rotated along the medial-lateral directions) and once along the sagittal plane (to generate models rotated along the dorsal-plantar directions). See Fig. 2 for a visual illustration.

To generate off-axis VOIs along the coronal plane (medial-lateral), the on-axis 0° 4.5 mm^3 VOI was rotated laterally within the larger 7.5 mm^3 VOI around its center of rotation by 10°, and a new VOI (denoted "C10°") was created. Thus, the axial and transverse axes of this new VOI, but not the radial axis, were rotated by 10° to the original principal axes of the bone. This 10 degree rotation was repeated nine times. Each time the VOI was rotated laterally by an additional 10°, until the original axial axis became the radial axis orientation (a final rotation of 90°). A total of nine laterally rotated VOIs were generated by increments of 10 degrees (denoted models C10°, C20°, C30°, C40°, C50°, C60°, C70°, C80° and C90° respectively, see Fig. 2 upper row).

To generate off-axis VOIs along the sagittal plane (dorsal-plantar), the same actions described above were repeated, this time rotating the on-axis 0° 4.5 mm^3 VOI dorsally by 10 degree increments. Thus, the axial and radial axes of the new VOI, but not the transverse axis, were rotated to the original principal axes of the bone. A total of nine dorsally rotated VOIs were generated by increments of 10 degrees (denoted models S10°, S20°, S30°, S40°, S50°, S60°, S70°, S80° and S90° respectively, see Fig. 2 lower row).

All 18 off-axis models were reconstructed (Amira 6.0) to create 3D surface models which were them saved in "stl" format and exported to our 3D printer.

2.6. Quantifying structural variation between models due to rotation

As a result of rotating the on-axis model by 10 degree increments up to 90° in two directions (laterally and dorsally) each of the 18 off-axis models covers slightly different bone volumes (i.e. by rotating the cubical VOI, previously included bone volume would be excluded, and an equal amount of new bone volume would be added). The only exceptions are the two off-axis 90 degrees models (C90° and S90°) as they are identical in volume and structure to the on-axis 0° model, yet the direction of printing and loading in these models is orthogonal to the original on-axis model. While the exclusion/addition of trabecular bone

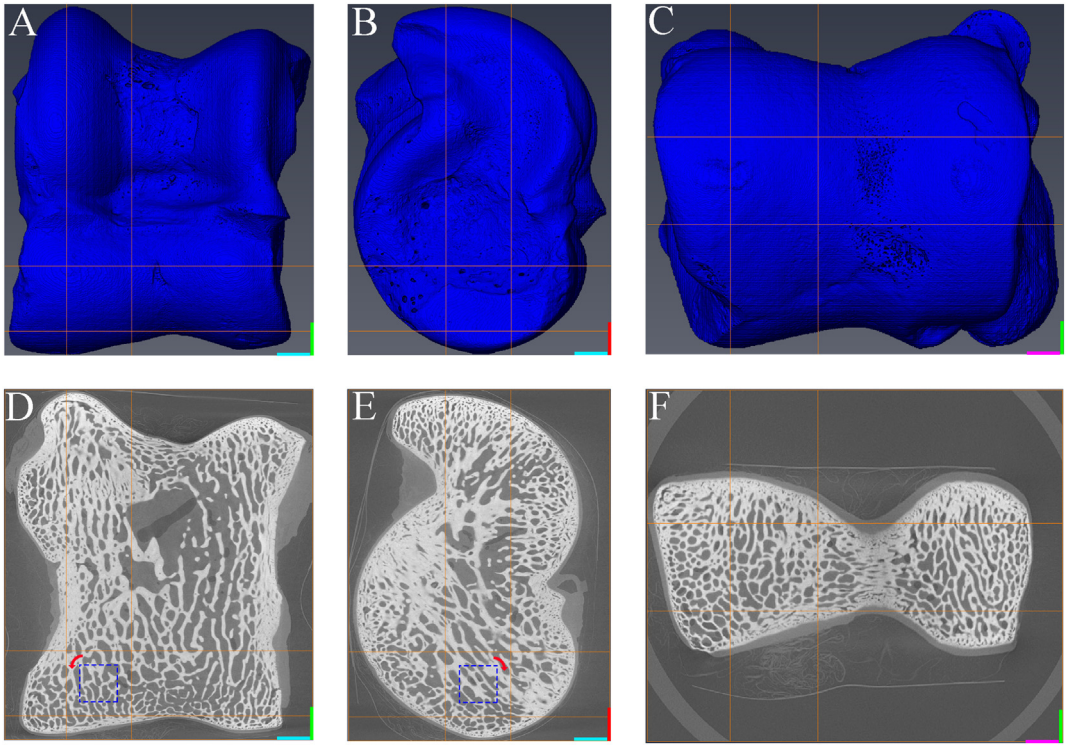

Fig. 1. Visualization of the talus used in the experiment. The 2D location of the 250 pixel^3 VOI (lateral side of the talus head) is marked in each panel by the intersecting orange lines. Bone orientation is color-coded at the right bottom corner of each panel: cyan marks inferior, light green marks medial, red marks dorsal and magenta marks plantar. A. Dorsal view. B. Lateral view. C. Inferior view. D. A cross-section along the coronal plane. The non-tilted 150 pixel^3 VOI is marked within the larger 250 pixel^3 VOI by a blue dashed square; the red arrow indicates the direction of the VOI tilting in the coronal plane – laterally. E. A cross-section along the sagittal plane. The non-tilted 150 pixel^3 VOI is marked within the larger 250 pixel^3 VOI by a blue dashed square; the red arrow indicates the direction of the VOI tilting in the sagittal plane – dorsally. F. A cross-section along the transverse plane. (For interpretation of the references to color in this figure legend, the reader is referred to the web version of this article.)

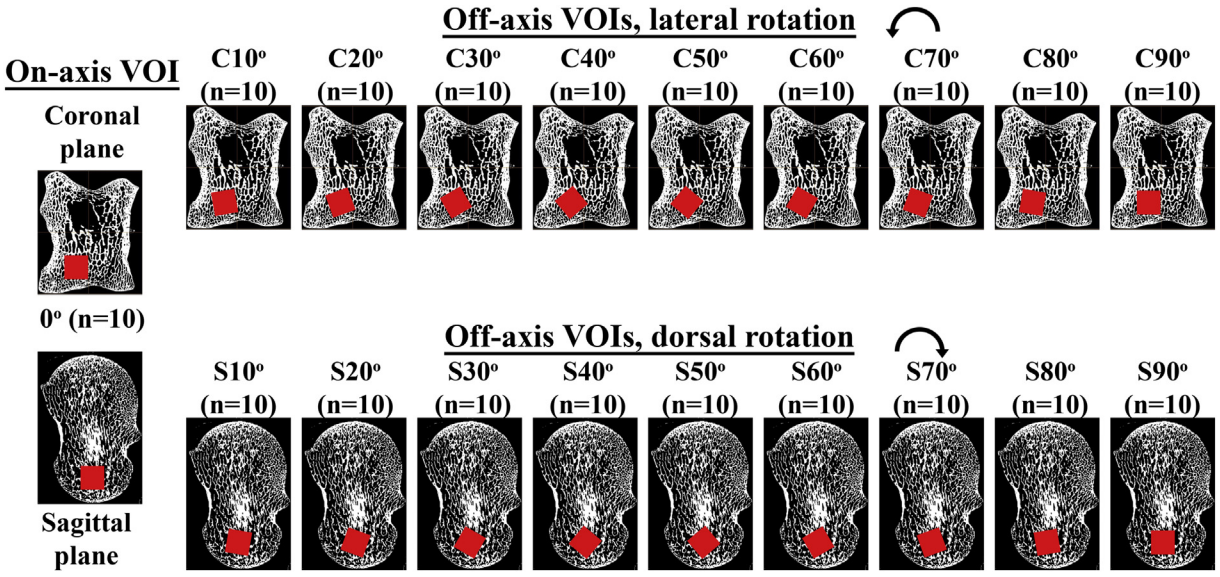

Fig. 2. On-axis and off-axis VOIs (depicted as red squares) and their location and orientation in the talus trabecular bone. Upper row of images shows the coronal plane of the talus, superior is up and lateral is left. Lower row of images shows the sagittal plane of the talus, superior is up and plantar is left. The on-axis VOI original location (red squares) is presented on the left side of the figure in both the coronal and sagittal planes. The nine off-axis VOIs that were generated when the on-axis VOI was rotated laterally along the coronal plane are presented in the upper row (red squares, C10° to C90°). The nine off-axis VOIs that were generated when the on-axis VOI was rotated dorsally along the sagittal plane are presented in the lower row (red squares, S10° to S90°). Note that both the C90° and the S90° models are identical to the on-axis 0° model in structure, yet the direction of printing (and mechanical loading) is orthogonal to the original on-axis model. Each VOI was 3D printed 10 times (n = 10) to a total of 190 3D printed replicas. (For interpretation of the references to color in this figure legend, the reader is referred to the web version of this article.)

volume is an inherent result of the rotation, it is important to quantify it. Our calculations revealed that the largest change happens in the first and last rotational steps (i.e. between the on-axis 0° model and the 10° off-axis model, and between the 80° and 90° off-axis models respectively), when a total of 7.34% of the old volume is excluded and an equal amount of new bone volume is added (see online supplementary material for a detailed explanation). Subsequent steps exclude/add decreasing amounts of bone volume – 5.01% between the 10° and 20°, and the 70° and 80° off-axis models, 3.12% between the 20° and 30°, and the 60° and 70° off-axis models, and 1.50% between the 30° and 40°, and the 50° and 60° off-axis models. The maximal cumulative excluded/added volume between the on-axis and off-axis models occurs at the 40° and 50° rotated models - 16.97% of the volume of these models does not exist in the 0° on-axis model. To verify that these differences in volume did not introduce any significant difference in structure, we have compared structural properties between all 19 models (see Section 2.8).

2.7. Isotropic model

To establish a reference for changes in the stiffness and strength of a porous 3D printed cubical model due to consecutive iterative rotations of its planes, we have fabricated a 3D isotropic cubic mesh made of beams in three orthogonal axes (Fig. 3). We predicted that loading such a structure on-axis (loading axis parallel to the direction of the beams) would yield higher stiffness and strength values when compared to the same isotropic model loaded off-axis (loading axis is at an angle to the direction of the beams). If our prediction for the isotropic model would be supported by the experimental results, any deviation from this behavior by the 3D printed trabecular structure (e.g. off-axis models stiffness and strength would not change or would be higher compared to the on-axis model) would imply that the trabecular structure we tested was truly not optimized to its primary physiological direction of loading, and not that a limitation of the 3D printing technique is responsible for this unexpected behavior.

Similarly to our trabecular bone model, we used Amira 6.0 to crop a 4.5 mm^3 VOI (150 $pixels^3$) from a larger fabricated isotropic structure; this smaller VOI served as the on-axis model (denoted I0°, Fig. 3). Such an isotropic structure has no a priori structural preference along any of its three principal axes. Next, we have rotated our 4.5 mm^3 VOI along its center of rotation by increments of 10° up to 40° and finally by an increment of 5° to a final rotation of 45°, by that creating five off-axis models (denoted models I10°, I20°, IC30°, I40° and I45° respectively, see Fig. 3). It is important to note that since our model was isotropic, any rotation larger than 45° would just mirror rotations smaller than 45° (e.g. the 40° model would be identical to the 60° model, etc.) and thus we have not fabricated any off-axis model with a rotation angle larger than 45°.

2.8. Verifying structural similarity between on-axis and off-axis models

To verify that the rotation of the on-axis trabecular model did not introduce any meaningful difference in trabecular structure, we have calculated bone volume fraction (BV/TV) and degree of anisotropy (DA) for the on-axis and 18 off-axis models. Each of the 19 models was saved as a stack of 2D bmp images and exported to BoneJ (version 1.4.2) for analysis [42]. Volume fraction was calculated as the ratio of "bone" to void voxels within the analyzed VOI. Degree of anisotropy was calculated using the mean intercept length (MIL) method where values of 0 and 1 represent a fully isotropic and anisotropic structure respectively. Calculations showed that the on-axis VOI had a volume fraction of 53.6% while the average volume fraction for the 18 off-axis VOIs was 53.6% ± 0.3% (values range between 53.0% - 54.2%). Similarly, the DA for the on-axis VOI was 0.80 and the average DA for the 18 off-axis VOIs was 0.77 ± 0.02 (values range between 0.72 and 0.80).

Similarly, to verify that the rotation of the on-axis isotropic model did not introduce any meaningful difference in structure, we have calculated the model volume fraction (BV/TV) for the on-axis and 5 off-axis models. The porosity of the on-axis isotropic model (I0°) was found to be 36.4%. Off-axis models had an average porosity of 36.2% ± 0.2% (values range between 36.0%–36.4%), revealing a maximum difference of < 1%. Finally, the on-axis model and the five off-axis models were reconstructed to create 3D surface models which were saved in "stl" format and exported to our 3D printer.

2.9. 3D printing

A total of 25 stl files were exported to our 3D printer software (3DPrint Client V1.1.128, 3DSystems Inc.), these included the 19 trabecular structure models (1 on-axis model, 9 sagittal off-axis models and 9 coronal off-axis models) and 6 fabricated isotropic models (1 on-axis model and 5 off-axis models). Each model was printed 10 times (4.5 × 4.5 × 4.5 mm, total $n = 250$) using a ProJet 1200 3D printer (3DSystems Inc.) and VisiJet FTX Green printing resin. VisiJet FTX Green is a UV curable plastic with a tension-compression strength asymmetry (similar to bone material) [43], an important feature that affects trabecular bone behavior especially during off-axis loading [20].

The ProJet 1200 3D printer uses a process called micro-Stereolithography (μSLA) to rapidly fabricate a 3D printed object. Briefly, this 3D printing process uses a UV laser source that projects a flash of light through a dynamic mask. The mask is the negative of the current 2D printed layer such that the UV light passes only where the object is solid and is blocked where voids exist. The UV light polymerizes the liquid photopolymer to create a part suspended from the build platform. The part is created layer after layer as the platform is elevated. One key advantage of μSLA over other 3D printing processes is its high spatial resolution (around 30 μm) and the quality of printing [44].

2.10. Validating accuracy and precision of 3D printing

Previously we have performed several tests to validate the accuracy and precision of our 3D printer [30,31]. In short, to test the accuracy of our printer (the ability to print correctly the segmented models), we have printed 4.5 × 4.5 × 4.5 mm cubes with various degrees of volume fraction (32.1%, 39.8% and 100% (i.e. solid)). Next, all printed cubes were weighed using a Vibra HT analytical balance with an accuracy up

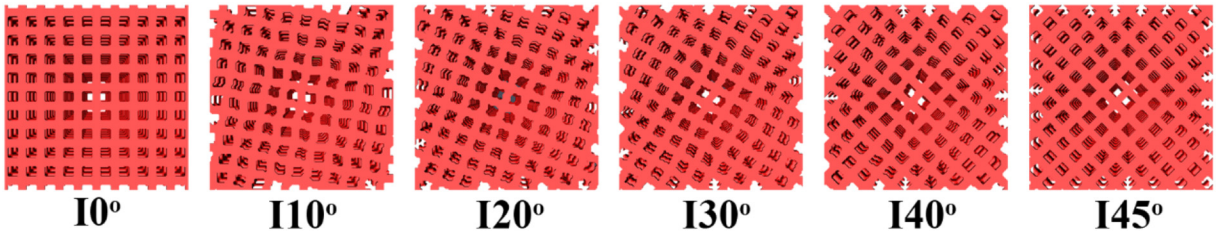

Fig. 3. Original on-axis 3D Isotropic cubic mesh (I0°) and the four rotated off-axis 3D Isotropic cubic meshes (I10° to I45°). The off-axis meshes were created by rotating the on-axis mesh along its center of rotation by increments of 10° up to 40° and finally by an increment of 5° to a final rotation of 45°.

to ± 0.0001 g (Vibra, Shinko Denshi *Co*. LTD). Finally, the average weight of the cubes was plotted against their volume fraction using the origin (0,0) as the fourth definite data point and a least squares linear regression was calculated. The weight of the printed cubes was found to significantly correlate with their volume fraction ($P < 0.01$; $R^2 = 0.9917$). To test the precision of our printer (the ability to repeatedly print the same segmented model), we have 3D printed a trabecular bone model at an initial size of 4.5 × 4.5 × 4.5 mm and then increasing all the way to 21 × 21 × 21 mm in increments of 1.5 mm (total of 12 cube sizes). Each cube size was printed three times and all cubes were weighed (Vibra, Shinko Denshi *Co*. LTD.). The max weight difference between the three cubes of each group size was < 3% (in most cases closer to 1%). Finally, the average weight of the 3D printed trabecular cubes was plotted against their volume and a least squares linear regression was calculated. The measured weight of the various cubes sizes was found to significantly correlate with their volume ($P < 0.01$; $R^2 = 0.9997$).

For the current study, all printed cubes were also weighed (Vibra, Shinko Denshi *Co*. LTD). The average weight of the 10 on-axis isotropic cubes was 96.7 mg ± 1.5 mg and the average weight of the fifty off-axis isotropic models was 96.3 mg ± 1.2 mg. The average weight of the 10 on-axis trabecular bone cubes was 64.1 mg ± 3.0 mg and the average weight of the 180 off-axis isotropic models was 64.9 mg ± 5.8 mg. In addition, printing accuracy was verified by measuring actual trabecular thickness for several trabeculae in one printed cube per group using a Nikon Eclipse E600 microscope. Measured values were compared to the expected thickness of the same trabeculae as given by the 3D segmented computer model. Average trabecular thickness difference between the models and printed cubes ranged between 2% to 5%. It is worth noting that a more precise measurement of actual trabecular thickness would be obtained by micro-CT scanning the 3D printed cubes, but this analysis was beyond the scope of the present study.

2.11. Mechanical testing

All 3D printed cubes were loaded until failure or up to 480 N (Load cell max load is limited to 500 N) using an Instron 5942 Single Column Table frame (Instron Inc., USA). All cubes were loaded in a direction that was perpendicular to the printed layers direction. As all 3D printed trabecular cubes failed before reaching our 480 N limit, we were able to measure for these samples both stiffness and strength. Some of the 3D printed isotropic cubes only yielded before reaching our 480 N limit (i.e. the stress-strain curve stopped behaving linearly but maximum load was not achieved) and thus we were only able to measure stiffness and yield strength (at 2% offset) for these samples.

Each cube was loaded at a rate of 50 μm/min (0.83 μm/s). To reduce shear stress due to friction between loading surfaces and samples we used low-friction polished stainless steel anvils and we applied a small preload (5 N) to 'tighten' the sample-anvil interface, before the experiment started. Only then load and deformation data were started to be collected (measurements were taken every 100 millisecond). The measured load and deformation were normalized by dividing their values with the cube area and height respectively to find the stress and strain. Next, a stress-strain curve was plotted for each test. Cube stiffness was determined from the linear region of the stress-strain curve. Strength, however, was less apparent due to the porous nature of our cubes. Contrary to solid samples, where strength is measured as the maximal stress the structure can sustain before failure (i.e. there is a clear point of peak stress), strength measurement in a porous structure, especially when porosity is relatively low, is less straight forward [45,46]. Fyhrie and Schaffler [45] have investigated the characteristic stress-strain curve of trabecular bone. They showed that when the first trabecula (or trabeculae) buckle and fail there is a drop in the stress-strain curve. Yet as more and more trabeculae fail, the specimen starts to collapse and the bone becomes compacted. At that stage, load (stress) may not change (or may even increase again) with the increase of deformation (denoted the "plateau region"). Thus, we have determined strength as the first point where load dropped > 1 N between two successive measurements. As measurements were recorded every 100 milliseconds and the anvil moved down at a speed of 0.83 μm/s, a drop of 1 N in 0.1 s would indicate a structural failure in our sample (i.e. buckling/failure of trabeculae).

2.12. Data analysis and statistics

To eliminate unintentional bias, all raw data files were assigned a random six-digit number and only then stiffness and strength (yield strength for the fabricated 3D printed isotropic cubes) were calculated. After the mechanical properties of all cubes were determined, file numbers were decoded and all files were regrouped with the other files of the same model. Statistical analyses were performed using R, version 3.2.0 [47]. Data (cubes' weights, stiffness and strength) were found to be distributed normally using the Shapiro test ($P > 0.05$). Population variances were found to be equal using the Bartllet test ($P > 0.05$). Statistical significant differences between the on-axis model and the off-axis models were calculated using an ANOVA test and a Dunnett's post-hoc test. Values smaller than 0.05 ($P < 0.05$) were considered to be statistically significant.

3. Results

3.1. Isotropic model stiffness and yield strength

The average stiffness and yield strength values with their standard deviations for the isotropic 3D printed models are given in Table 1. There is a clear trend of decrease in stiffness and yield strength as we move from the I0° on-axis model (elements are parallel to the direction of loading) to the off-axis models (stiffness and yield strength gradually decrease as angle of rotation increases, I10° to I45°, see Table 1).

Average stiffness for the on-axis model is 299.5 ± 107.8 MPa compared with 235.2 ± 135.6 MPa for the group of off-axis models combined. When comparing the on-axis model stiffness value to each of the off-axis models separately (Table 1), I0° on-axis stiffness was significantly higher than the off-axis stiffness for models I30°, I40° and I45° ($P < 0.05$). The off-axis stiffness for the I10° model was close to significantly higher (just slightly above 0.05) compared to the off-axis stiffness for models I30°, I40° and I45°. No other in-between model stiffness values were found to be significantly different.

Average yield strength for the I0° on-axis model is 18.0 ± 2.4 MPa compared with 14.0 ± 3.8 MPa for the group of off-axis models combined. When comparing the I0° on-axis model yield strength value to each of the off-axis models separately (Table 1), on-axis yield strength was non-significantly different from the I10° off-axis model, but both the on-axis and the I10° off-axis models demonstrated significantly higher yield strength values in comparison to all other off-axis models (I20°, I30°, I40° and I45°; $P < 0.05$). No significant difference in yield strength values was found between the I20°, I30°, I40° and I45° models ($P \geq 0.05$).

Table 1
Stiffness and yield strength results for the on-axis and off-axis isotropic 3D printed models.

	Stiffness MPa (SD)	Yield strength MPa (SD) at 2% offset
I0° (on-axis)	299.5 (107.8)	18.0 (2.4)
I10°	288.3 (169.0)	16.7 (4.9)
I20°	269.2 (145.2)	13.4 (3.3)
I30°	205.7 (84.8)	13.2 (2.9)
I40°	223.7 (108.5)	13.0 (2.2)
I45°	199.6 (165.5)	13.2 (4.1)

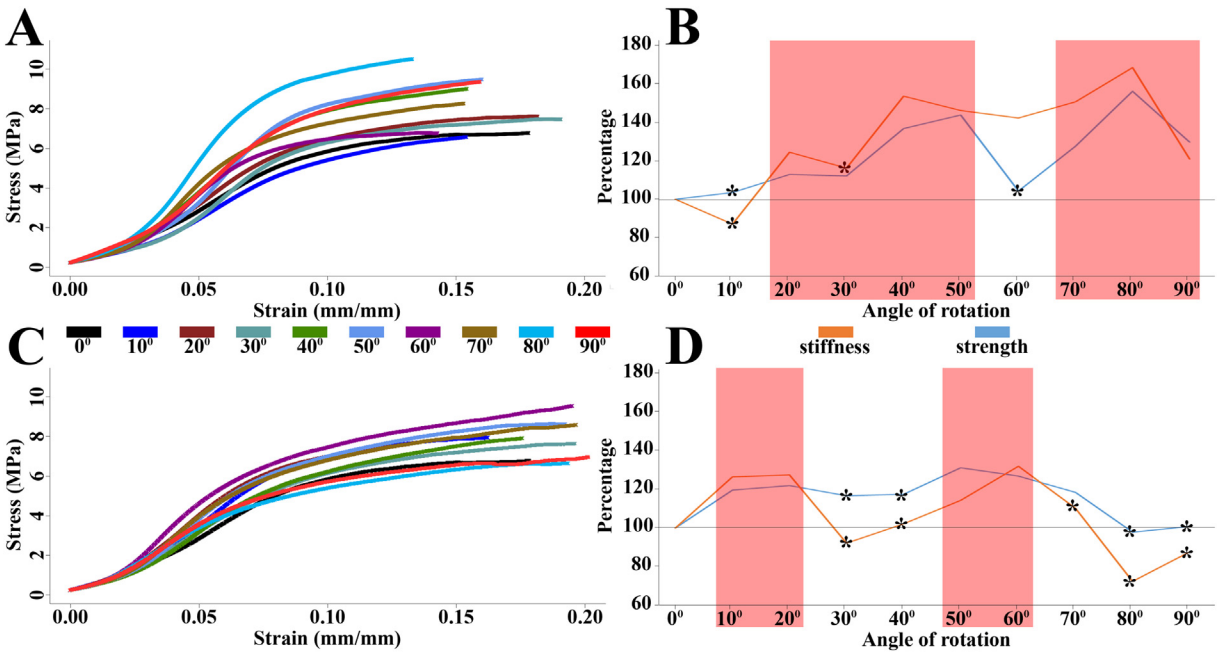

Fig. 4. Average stress-strain curves (A and C, left side) and average relative stiffness and strength values (B and D, right side) for the on-axis model and off-axis models rotated laterally (A and B, upper row) and dorsally (C and D, lower row). All off-axis stiffness and strength values are relative to the stiffness and strength values of the on-axis model which is depicted as 100% (i.e. a stiffness value of 120% indicates a 20% increase in stiffness for that off-axis model). Values denoted with an asterisk are non-significantly different than the stiffness or strength values for the on-axis model. Areas shaded in red represent off-axis models with significantly higher stiffness and strength values compared to the on-axis model. Color codes for the 10 different models (0° to 90°, left side) and for stiffness and strength values (right side) are between the two rows of images. (For interpretation of the references to color in this figure legend, the reader is referred to the web version of this article.)

3.2. Trabecular models stiffness and strength

Average stress-strain curves and the corresponding stiffness and strength values for the 0° on-axis model and the off-axis models rotated in the coronal (laterally) and sagittal (dorsally) planes are given in Fig. 4 and Tables 2 and 3.

In general, the on-axis trabecular structure demonstrated lower stiffness and strength values when compared to the off-axis trabecular structures. This observation is correct for both the laterally and dorsally rotated off-axis trabecular structures, yet the differences are more pronounced for the laterally rotated off-axis trabecular structures (Fig. 4 upper vs. lower row). The average stiffness for the 0° on-axis trabecular structure was 103.7 ± 19.5 MPa, compared with 139.5 ± 36.2 MPa and 111.2 ± 30.8 MPa for the laterally and dorsally rotated off-axis trabecular structures respectively. The average strength for the 0° on-axis trabecular structure was 6.5 ± 0.7 MPa, compared with 8.1 ± 1.3 MPa and 7.6 ± 1.1 MPa for the laterally and dorsally rotated off-axis trabecular structures respectively.

Laterally rotated off-axis trabecular structures (off-axis models C10° to C90°) demonstrated persistent significantly higher stiffness and strength values in comparison to the on-axis trabecular structure ($P < 0.05$) (Fig. 4A and B, and Table 2). Laterally rotated off-axis trabecular structures with significantly elevated stiffness and strength values are shaded (red) in Fig. 4B. The only exceptions were models C10° and C30°, which demonstrated non-significant differences from the on-axis trabecular structure stiffness, and models C10° and C60°, which demonstrated non-significant differences from the on-axis trabecular structure strength. Dorsally rotated off-axis trabecular structures (off-axis models S10° to S90°) also demonstrated significantly higher stiffness and strength values in comparison to the on-axis trabecular structure ($P < 0.05$) (Fig. 4C and D, and Table 3), yet these differences were not as distinct or as constant as for the laterally rotated off-axis trabecular structures. Compared to 0° on-axis trabecular structure stiffness, the stiffness values for the dorsally rotated off-axis trabecular structures were significantly higher for the S10° and S20°, and for the S50° and S60° models ($P < 0.05$) (Fig. 4D). The strength values for the dorsally rotated off-axis trabecular structures demonstrated a similar behavior to the stiffness values and were significantly

Table 2
Stiffness and strength results for the on-axis and laterally rotated off-axis models.

	Stiffness MPa (SD)	Strength MPa (SD)
C0° (on-axis)	103.7 (19.5)	6.5 (0.7)
C10°	90.2 (20.1)	6.7 (0.6)
C20°	129.2 (28.8)	7.3 (0.7)
C30°	120.5 (20.2)	7.3 (0.5)
C40°	159.4 (39.8)	8.9 (0.5)
C50°	151.8 (42.7)	9.3 (0.6)
C60°	147.7 (16.2)	6.8 (0.3)
C70°	156.3 (14.4)	8.3 (0.7)
C80°	174.9 (31.9)	10.1 (0.8)
C90°	125.6 (24.3)	8.4 (0.8)

Table 3
Stiffness and strength results for the on-axis and dorsally rotated off-axis models.

	Stiffness MPa (SD)	Strength MPa (SD)
S0° (on-axis)	103.7 (19.5)	6.5 (0.7)
S10°	131.2 (19.2)	7.8 (0.5)
S20°	132.2 (24.5)	7.9 (0.8)
S30°	95.6 (31.6)	7.6 (0.4)
S40°	106.0 (20.5)	7.6 (1.5)
S50°	118.7 (38.1)	8.5 (1.0)
S60°	136.9 (19.9)	8.2 (1.1)
S70°	114.3 (31.6)	7.7 (1.5)
S80°	75.1 (10.3)	6.3 (0.6)
S90°	91.0 (11.2)	6.5 (0.7)

higher in comparison to the on-axis trabecular structure for the S10° and S20°, and for the S50°, S60° and S70° models ($P < 0.05$; Fig. 4D). Dorsally rotated off-axis trabecular structures with significantly elevated stiffness and strength values are shaded (red) in Fig. 4D.

4. Discussion

The major objective of this study was to support Wilhelm Roux's principle of bone functional adaptation for the first time in a direct way. As Roux's principle of bone functional adaptation predicts bone deposition and resorption in response to mechanical stimuli (i.e. bone modeling), it is expected that the outcome of bone modeling will be a structure that is now better adapted to its function. Therefore, it is postulated that a modeled trabecular structure is stiffest and strongest in line with the direction of mechanical stimuli as it is transmitted from one cortex to the other, and that mechanical stiffness and strength will diminish as we move away from this loading orientation. However, since each trabecular structure is unique and since trabecular structure can only be loaded once before it is damaged, so far a direct test of this hypothesis was unattainable. To address this issue, we have used a 3D printing process called μSLA to reproduce multiple accurate replicas of a modeled trabecular bone structure cropped from a sheep talus in various angles to the principal direction of physiological loading. These replicas were loaded in compression until failure and their stiffness and strength values were recorded. If Roux's principle of bone functional adaptation is correct, we will expect the on-axis replica (cropped parallel to the 3 principal axes of the bone) to demonstrate the highest stiffness and strength values in comparison to the off-axis replicas (cropped in angles incrementing by 10°, from 10° to 90° to the 3 principal axis of the bone). Contrary to our prediction, and in disagreement with Roux's principle of bone functional adaptation, we found that a trabecular structure loaded off-axis tended to have higher stiffness and strength values when compared to the same trabecular structure loaded on-axis. These unexpected results may not directly refute Roux's principle of bone functional adaptation but they do raise questions as to whether this principle applies equally to all bones and whether its sole purpose is to adapt bone structure to the principal physiological direction of loading.

So far, very few *in silico* FE models looked at the mechanical properties of a single trabecular structure both on- and off-axis. Van Rietbergen et al. [48] used FEA to calculate the nine elastic constants of an orthotropic trabecular sample with a BV/TV of 35% from a whale vertebral body. The model was tested twice, once 45° to the body longitudinal axis and then again after an optimization procedure was used to reorient the model along its three orthotropic fabric axes. Similar to our study, they have found that the stiffness along the direction of loading was higher when the sample was loaded at 45° to the body longitudinal axis then when it was oriented along the principal trabecular direction. As no previous study tested in vitro the mechanical properties of a single trabecular structure both on-axis and off-axis, we are restricted in comparing our results to the few previous studies that mechanically tested various trabecular bone samples from adjacent regions, some on-axis and others off-axis [49–54]. Accordingly, these studies never demonstrated that on-axis mechanical properties are superior to off-axis mechanical properties for a given unique structure. Chang et al. [54] tested in compression cylindrical trabecular bone samples from bovine proximal tibiae. Some of the samples were prepared on-axis while others were machined off-axis (30–40° oblique to on-axis). Their results revealed similar yield strain values for the on- and off-axis loadings but a decrease of around 30% in stiffness when samples were loaded off-axis [54]. In a similar study, Ohman et al. [50] tested in compression cylindrical trabecular bone samples from human femoral heads. Ten cylinders were extracted on-axis, along the main direction of trabecular bone and additional ten cylinders were extracted off-axis, with a misalignment of approximately 20° to the trabecular main direction. No significant differences were found in structural parameters and ash content between the two groups, yet the off-axis group demonstrated a significant decrease in stiffness and strength (around 40%) [50]. While these values were statistically significant, it is worth mentioning that the main direction of trabecular bone was determined from 2D images. Thus, the main direction of trabecular bone could only be determined along an arbitrary plane of the image and not in the entire 3D volume. In addition, main trabecular direction was determined by an observer and the authors assumed an additional error of up to 10°. In contrast to the above results, Birnbaum et al. [53] found no significant difference in strength when parallelepiped trabecular bone samples from human femoral head were tested parallel, perpendicular and at 45° to the main trabecular direction. Furthermore, Bevill et al. [49] cored fifty cylindrical samples from human lumbar vertebral bodies and femoral necks. Twenty-two of the samples were cut with the cylinder axis aligned along the principal trabecular orientation (i.e. on-axis) and twenty-eight samples were prepared with the cylinder axis at an oblique angle of 15° or 45° to the principal trabecular orientation (i.e. off-axis). Their results revealed a significant decrease in stiffness between the on-axis and 45° off-axis group for the femoral neck samples but not the lumbar vertebrae [49], implying variable adaptation depending on the type of bone. When they simulated their mechanical testing using finite element analysis they found that less trabeculae failed in the vertebral body, probably due to substantial bending deformations that occurred before failure. These inconclusive results, obtained from studies that were testing various trabecular bone samples on- and off-axis, exemplify the limitation of this approach [55]. The large structural variation and consequently the mechanical properties variation within any bone volume makes the assumption that samples taken adjacent to each other at different orientations to the principal axis will have identical properties unlikely.

Additional comparison can be made between our study and previous studies that tested trabecular bone samples along their 3 principal axes (superior-inferior or caudal-cranial, lateral-medial and anterior-posterior), as their perpendicular loading to the principal axis correspond to our 90° dorsal and lateral rotation models. However, the majority of these studies either estimated stiffness in different orientations from ultrasound measurements (i.e. not an actual mechanical testing) [56–60] or mechanically tested three groups of trabecular samples (and thus different structures), each along a different principal axis [61–71]. Although most studies that tested trabecular bone samples from long bones (e.g. femur and tibia) revealed significantly higher stiffness and strength when samples were loaded along the principal axis of loading compared to the two perpendicular directions [61–64,67–69], some showed opposite trends [53,65,72]. On the other hand, most studies that tested trabecular bone samples from short or irregular bones (e.g. vertebrae and patella, similar to the talus in our study) showed that loading along orientations that were orthogonal to the principal axis demonstrated non-significant differences or even significantly higher stiffness and strength values [57,61,62,66]. Both Augat et al. [61] and Majumdar et al. [62] found that calcaneal trabecular samples behaved mechanically different than samples taken from the proximal and distal femur. While Majumdar et al. [62] did find stiffness differences between the 3 principal axes, these differences were much smaller compared to the samples from the femur. Augat et al. [61], found that contrary to the femoral trabecular samples, calcaneal samples demonstrated close to isotropic behavior with a tendency for higher stiffness values along the anterior-posterior direction. Cavani et al. [57] also found isotropic behavior when they used ultrasound to estimate the stiffness of equine thoracic vertebrae. Finally, Townsend et al. [66] showed that trabecular bone cubes from human patella demonstrated the lowest stiffness along the lateral-medial direction and the highest stiffness along the anterior-posterior direction and not the expected proximal-distal direction (yet the stiffness values along these two directions were relatively similar). These results may indicate that while long bones “obey” Roux's principle of bone functional adaptation and adjust their trabecular structure to support

predominantly uniaxial loading, this process is inexplicit in bones with less clear uniaxial loading [73] or regions that lack organized growth plates and thus their trabecula are not formed in perpendicular direction to the long axis of the bone (like the talus in our study).

There may be other possible explanations to why trabecular structures demonstrate a tendency for higher stiffness and strength during off-axis loading. Several studies have suggested that trabecular bone behaves and fails differently when it is loaded on-axis vs. off-axis or perpendicular to the principal axis [49,68,74] and that this behavior differs between bone areas with low- versus high-density (the BV/TV of our talus VOI was 53.6%) [49,75]. While trabeculae that are loaded parallel to the principal trabecular direction tend to be shielded from buckling by supporting horizontal trabeculae and thus tend to fail in shear [74], loads applied normal or at an angle to the principal trabecular direction tend to cause bending in trabeculae before they buckle and fail [49,68]. Since we have determined strength as a drop of 1 N between 2 consecutive measurements (time difference of 0.1 s) our method was probably more sensitive in detecting trabeculae failing in shear (catastrophic failure that leads to a sudden drop in force) than failure due to increase in bending (gradual drop in force). A second explanation relates to microstructural differences along different trabecular orientations. While we were able to show that BV/TV and DA did not differ between the on- and off-axis VOI's, we did not account for additional structural differences (Tb.Th, Tb.N and rod vs. plate) between horizontal and vertical trabeculae. Seeing that our BV/TV was relatively high (53.6%), it is safe to predict that many of the trabecula in our VOI were plate in nature. If more trabecular plates are aligned in horizontal and oblique planes compared to the vertical plane this would not decrease DA, yet we would see an increase in stiffness and strength when we will load the sample along these orientations. A third explanation is that our trabecular sample was cropped from a short bone – the talus. As was mentioned above, contrary to long bones, short bones tend to show either isotropic mechanical behavior or higher stiffness and strength when the tissue is loaded off-axis or perpendicular to the principal direction of loading. As the talus is lacking a growth plate and thus it ossifies solely via ossification centers [36,37], the trabecular structure is not initially oriented perpendicular to the long axis of the bone and thus the mechanical behavior may vary from our predications which are based on a typical long bone that possesses a growth plate. A fourth possible explanation relates to the evidence that different regions in a specific bone may model and adjust to different loading scenarios (uniaxial vs. multiaxial loading). Several previous studies have demonstrated both isotropic and orthotropic mechanical behaviors of trabecular bone samples and higher stiffness and strength values along different orientations, depending on samples' location within the bone and the way they were loaded in vivo [65,67]. Martens et al. [65] mechanically tested cubical trabecular bone samples along their 3 principal axes, taken from the head, neck and intertrochanteric regions of human femora. They have noted differences in mechanical behavior between the different regions. While samples from the femoral head and intertrochanteric regions demonstrated transverse isotropic behavior (with different orientations having the highest stiffness and strength), the neck region demonstrated a clear orthotropic behavior [65]. Similarly, Ciarelli et al. [67] noted that mechanical properties of human trabecular samples tended to vary between bones and locations, and to correspond with their functional demands. For example, samples from the femoral head tended toward isotropic mechanical behavior while samples from the distal femur appeared to be more transverse isotropic along the sagittal plane. This correlated well with the need of the distal femur to withstand stresses over an extended range of flexion angles [67]. A similar mechanism of extended range of in vivo loading angles may account for the higher stiffness and strength values we have observed during off-axis loading. Our trabecular bone sample was cropped from the distal talus, just under the talus head (Fig. 1). The ankle joint of ungulate mammals can dorsiflex and plantarflex quite substantially during trotting or running and thus it is expected that high stresses will be experienced over a range of angles along the talus head. Consequently, higher stiffness and strength along a range of angles in the sagittal plane (dorsal rotation) is beneficial. Furthermore, since the ankle joint is situated rather distally, close to the contact point with the surface, where ground reaction forces are generated, stresses are expected to be fairly high. As the talus has no muscle attachments to its surface and no big muscles nearby to protect it, its trabecular structure may also be subjected to a range of loading angles along the lateral-medial orientation due to slight inversion and eversion of the hoof as its contacting the ground. Thus, somewhat higher stiffness and strength along a range of angles in the coronal plane (lateral rotation) is also beneficial. A fifth explanation is that trabecular bone is just one load-carrying element in the interconnected mechanical system of cortical and trabecular bone tissues. In that sense, trabecular structure adjusts in response to mechanical stimuli to better transmit loads between the bone cortices. Yet this does not require the trabecular component to be the stiffest and strongest in that direction, but rather the interconnected system of trabecular and cortical bone as a whole. Thus, the bone organ may gain much more from trabecular structure that is stiffer and stronger during off-axis loading (e.g. a fall) because that's a direction where the whole bone is less optimized to support against unexpected high impact forces. In line with this idea, de Bakker et al. [76] noted that in the human femoral neck, maximal compressive stresses were switched from the inferior aspect during normal loading to the superolateral aspect during sideways falls. They suggested that trabecular bone may reinforce cortical bone by decreasing the effective length of superior cortex sections when the femur experiences compressive stress due to bending, secondary to impact force on the greater trochanter in a fall [75] (i.e. off-axis loading). One final possibility, that we must recognize, to our unexpected results relates to some potential inherent limitations of the 3D printing technique itself. As our 3D printed model is fabricated from a micro-CT scan, 3D printing or micro-CT scanning resolution issues can affect how accurate our printed replicas represent the real trabecular bone structure. Furthermore, the use of a homogenous and isotropic 3D printing resin excludes any mechanical contribution the inhomogeneous, anisotropic and hierarchical bone material would have on the actual trabecular structure. Consequently, this may change the yield and post-yield behavior of our models in comparison to the behavior of the original bone sample.

While our study yielded new and interesting findings, they must be assessed in light of the study's limitations. The main limitation of this study is that we only used one trabecular bone structure from one bone. This is a direct result of the huge amount of time and work involved in segmenting and creating all the on- and off-axis models, 3D printing 250 replicas and then mechanically test them. Nevertheless, we found that off-axis loading tended to yield higher stiffness and strength values in both rotation scenarios and in most of the 18 off-axis models. Furthermore, to verify that our results are not affected by our experimental setup (namely the 3D printer) we fabricated, 3D printed and mechanically tested an isotropic structure. The fact that this isotropic structure performed mechanically as expected (i.e. highest stiffness and strength when loaded on-axis and diminishing stiffness and strength values as we move off-axis) and contrary to out trabecular replica (in both rotation scenarios), supports the validity of our results. In addition, since no study yet was able to directly support Roux's principle of bone functional adaptation we believe that this one refuting example is important. Hence, we believe that our unexpected findings are supported and that they bring new understandings that deserve further investigations. Currently we are working on a follow-up study, to quantify the distribution of stresses and strains in our VOI during on- and off-axis loading using an FE model. Another possible limitation of our study is that our replicas only represent the bone structure but not its material. Thus, our replicas are a macro representation of the bone structure without any of the micro and nano structures (e.g. lamellae, lacunae and mineralized collagen fibrils). However, this is an inherent limitation of our technique that is shared to some degree with another

tool that is widely used in bone biomechanics research – FEA. While some aspects of bone behavior may be altered by these missing details, FEA models were shown to replicate reliably bone biomechanical behavior even when this information was missing. One more limitation of this study, one that is common to almost all other studies that mechanically test trabecular bone samples, is that we tested the trabecular structure alone, "detached" from the neighboring trabecula (i.e. we created new edges and severed trabeculae) and the enclosing cortical bone. Since in vivo cortical and trabecular bone tissue are a continuum and mechanical loads are transmitted from one to the other, dichotomizing these two components may alter the way each of them is behaving separately. Finally, the relatively high stiffness standard deviation values for the talus and the isotropic model are yet another potential limitation. This is a direct outcome of 3D printing very thin trabeculae. Small, uncontrolled variations in printing output, will have a larger effect on stiffness (structure deformation) than on strength (max loading). Nevertheless, seeing that stiffness and strength values follow a very similar trend of increased values in specific off-axis angles (see Fig. 4), and the fact that despite the high SDs stiffness differences are still statistically significant for these angles, imply that these differences cannot be ignored or dismissed as random or erroneous.

5. Conclusions

The goal of this study was to find direct support to Roux's principle of bone functional adaptation. We hypothesized that a modeled trabecular bone structure will demonstrate higher mechanical stiffness and strength when it is loaded along the principal direction of physiological loading, in comparison to when it is loaded off-axis. Contrary to our prediction, and opposing Roux's principle of bone functional adaptation, we found that a trabecular structure loaded off-axis tended to have higher stiffness and strength values when compared to the same trabecular structure loaded on-axis. These unpredictable findings imply that trabecular bone adaptation may serve additional purposes than simply optimizing bone structure to one principal loading scenario and they suggest that we still do not understand bone modeling to its entirety.

Declaration of competing interest

The authors have no conflicts of interest to declare.

Acknowledgments

For funding, the authors thank Winthrop University Research Council Grant SC15013 and SC INBRE grants from the National Institute of General Medical Sciences (8 P20 GM103499) of the National Institutes of Health. A special thanks to Dr. Zach and Kristen Abernathy from the Department of Mathematics at Winthrop University for helping with calculations. Thanks are also owed to the Associate Editor and two anonymous reviewers for their helpful comments that considerably improved this manuscript. Dr. Meir Barak would like to personally acknowledge Dr. John D. Currey for his mentorship, friendship and help through the years, he will be missed.

Authors' contributions

Zach Wood: Conceptualization, Methodology, Formal Analysis, Investigation, Writing – Original Draft, Writing – Review & Editing, Visualization. **Lisa Lynn:** Conceptualization, Methodology, Formal Analysis, Investigation, Writing – Original Draft, Writing – Review & Editing, Visualization. **Jack Nguyen:** Validation, Formal Analysis, Writing – Review & Editing. **Arielle Black:** Methodology, Validation, Formal Analysis, Investigation, Writing – Review & Editing. **Meha Patel:** Methodology, Validation, Formal Analysis, Investigation, Writing – Review & Editing, Visualization. **Meir M. Barak:** Conceptualization, Formal Analysis, Writing – Original Draft, Writing – Review & Editing, Visualization, Supervision.

Appendix A. Supplementary data

Supplementary data to this article can be found online at https://doi.org/10.1016/j.bone.2019.08.002.

References

[1] J.D. Currey, Bones: Structure and Mechanics, 2nd ed., Princeton University press, Oxford, 2002.
[2] J. Wolff, The Law of Bone Remodelling, Springer-Verlag, Berlin Heidelberg, 1986.
[3] S.C. Cowin, The false premise in Wolff's law, Bone Mechanics Handbook, 2nd ed., CRC Press, 2001, pp. 30–31–30–15.
[4] R. Huiskes, If bone is the answer, then what is the question? J. Anat. 197 (2000) 145–156, https://doi.org/10.1046/j.1469-7580.2000.19720145.x.
[5] J.D. Currey, The many adaptations of bone, J. Biomech. 36 (2003) 1487–1495, https://doi.org/10.1016/S0021-9290(03)00124-6.
[6] M.M. Barak, D.E. Lieberman, D. Raichlen, H. Pontzer, A.G. Warrener, J.-J. Hublin, Trabecular evidence for a human-like gait in Australopithecus africanus, PLoS One 8 (2013) e77687, , https://doi.org/10.1371/journal.pone.0077687.
[7] M.M. Barak, D.E. Lieberman, J.-J. Hublin, A Wolff in sheep's clothing: trabecular bone adaptation in response to changes in joint loading orientation, Bone 49 (2011) 1141–1151, https://doi.org/10.1016/j.bone.2011.08.020.
[8] M.M. Barak, E. Sherratt, D.E. Lieberman, Using principal trabecular orientation to differentiate joint loading orientation in the 3rd metacarpal heads of humans and chimpanzees, J. Hum. Evol. 113 (2017) 173–182, https://doi.org/10.1016/j.jhevol.2017.08.018.
[9] T.L. Kivell, A review of trabecular bone functional adaptation: what have we learned from trabecular analyses in extant hominoids and what can we apply to fossils? J. Anat. 228 (2016) 569–594, https://doi.org/10.1111/joa.12446.
[10] M.M. Skinner, N.B. Stephens, Z.J. Tsegai, A.C. Foote, N.H. Nguyen, T. Gross, D.H. Pahr, J.-J. Hublin, T.L. Kivell, Human evolution. Human-like hand use in Australopithecus africanus, Science 347 (2015) 395–399, https://doi.org/10.1126/science.1261735.
[11] T.M. Ryan, C.N. Shaw, Unique suites of trabecular bone features characterize locomotor behavior in human and non-human anthropoid primates, PLoS One 7 (2012) e41037, , https://doi.org/10.1371/journal.pone.0041037.
[12] M.M. Barak, S. Weiner, R. Shahar, Importance of the integrity of trabecular bone to the relationship between load and deformation of rat femora: an optical metrology study, J. Mater. Chem. 18 (2008) 3855–3864.
[13] M.M. Barak, S. Weiner, R. Shahar, The contribution of trabecular bone to the stiffness and strength of rat lumbar vertebrae, Spine 35 (2010) E1153–E1159, https://doi.org/10.1097/BRS.0b013e3181e5e34b.
[14] S.K. Eswaran, A. Gupta, M.F. Adams, T.M. Keaveny, Cortical and trabecular load sharing in the human vertebral body, J. Bone Miner. Res. 21 (2006) 307–314, https://doi.org/10.1359/jbmr.2006.21.2.307.
[15] M. Ito, A. Nishida, A. Koga, S. Ikeda, A. Shiraishi, M. Uetani, K. Hayashi, T. Nakamura, Contribution of trabecular and cortical components to the mechanical properties of bone and their regulating parameters, Bone 31 (2002) 351–358.
[16] H. Pontzer, D.E. Lieberman, E. Momin, M.J. Devlin, J.D. Polk, B. Hallgrímsson, D.M.L. Cooper, Trabecular bone in the bird knee responds with high sensitivity to changes in load orientation, J. Exp. Biol. 209 (2006) 57–65, https://doi.org/10.1242/jeb.01971.
[17] F. Linde, I. Hvid, N.C. Jensen, Material properties of cancellous bone in repetitive axial loading, Eng. Med. 14 (1985) 173–177.
[18] F. Linde, I. Hvid, Stiffness behaviour of trabecular bone specimens, J. Biomech. 20 (1987) 83–89.
[19] R. Shahar, P. Zaslansky, M. Barak, A.A. Friesem, J.D. Currey, S. Weiner, Anisotropic Poisson's ratio and compression modulus of cortical bone determined by speckle interferometry, J. Biomech. 40 (2007) 252–264.
[20] G. Bevill, T.M. Keaveny, Trabecular bone strength predictions using finite element analysis of micro-scale images at limited spatial resolution, Bone 44 (2009) 579–584, https://doi.org/10.1016/j.bone.2008.11.020.
[21] C. Boyle, I.Y. Kim, Three-dimensional micro-level computational study of Wolff's law via trabecular bone remodeling in the human proximal femur using design space topology optimization, J. Biomech. 44 (2011) 935–942, https://doi.org/10.1016/j.jbiomech.2010.11.029.
[22] P. Christen, B. van Rietbergen, F.M. Lambers, R. Müller, K. Ito, Bone morphology allows estimation of loading history in a murine model of bone adaptation, Biomech. Model. Mechanobiol. 11 (2012) 483–492, https://doi.org/10.1007/s10237-011-0327-x.
[23] W.C.H. Parr, U. Chamoli, A. Jones, W.R. Walsh, S. Wroe, Finite element micro-modelling of a human ankle bone reveals the importance of the trabecular network to mechanical performance: new methods for the generation and comparison of 3D models, J. Biomech. 46 (2013) 200–205, https://doi.org/10.1016/j.jbiomech.2012.11.011.
[24] M.M. Barak, S. Geiger, N.L.-T. Chattah, R. Shahar, S. Weiner, Enamel dictates whole tooth deformation: a finite element model study validated by a metrology method, J. Struct. Biol. 168 (2009) 511–520, https://doi.org/10.1016/j.jsb.2009.07.019.
[25] C.A. Dobson, G. Sisias, R. Phillips, M.J. Fagan, C.M. Langton, Three dimensional stereolithography models of cancellous bone structures from μCT data: testing and

validation of finite element results, Proc. Inst. Mech. Eng. H J. Eng. Med. 220 (2006) 481–484, https://doi.org/10.1243/09544119H00405.
[26] V. kuhn, N. Ivanovic, W. Recheis, High resolution 3D-printing of trabecular bone based on micro-CT data, J. Orthop. Transl. 2 (2014) 238.
[27] C.M. Langton, M.A. Whitehead, D.K. Langton, G. Langley, Development of a cancellous bone structural model by stereolithography for ultrasound characterisation of the calcaneus, Med. Eng. Phys. 19 (1997) 599–604.
[28] B.C. Tellis, J.A. Szivek, C.L. Bliss, D.S. Margolis, R.K. Vaidyanathan, P. Calvert, Trabecular scaffolds created using micro CT guided fused deposition modeling, Mater. Sci. Eng. C Mater. Biol. Appl. 28 (2009) 171–178, https://doi.org/10.1016/j.msec.2006.11.010.
[29] Y.-J. Yoon, S.K. Moon, J. Hwang, 3D printing as an efficient way for comparative study of biomimetic structures — trabecular bone and honeycomb, J. Mech. Sci. Technol. 28 (2014) 4635–4640, https://doi.org/10.1007/s12206-014-1031-4.
[30] M.M. Barak, A.M. Black, Using 3D-printing to evaluate trabecular bone mechanical properties, FASEB J. 31 (2017) (902.23-902.23).
[31] M.M. Barak, M.A. Black, A novel use of 3D printing model demonstrates the effects of deteriorated trabecular bone structure on bone stiffness and strength, J. Mech. Behav. Biomed. Mater. 78 (2018) 455–464, https://doi.org/10.1016/j.jmbbm.2017.12.010.
[32] P. Mc Donnell, N. Harrison, S. Lohfeld, O. Kennedy, Y. Zhang, P.E. Mc Hugh, Investigation of the mechanical interaction of the trabecular core with an external shell using rapid prototype and finite element models, J. Mech. Behav. Biomed. Mater. 3 (2010) 63–76, https://doi.org/10.1016/j.jmbbm.2009.03.002.
[33] M. Cima, E. Sachs, L. Cima, J. Yoo, S. Khanuja, S. Borland, B. Wu, R. Giordano, Computer-derived micro-structures by 3D printing: bio- and structural materials, Proceedings of the SFF Symposium, 1994, pp. 181–190.
[34] E. Sachs, M. Cima, J. Cornie, Three-dimensional printing: rapid tooling and prototypes directly from a CAD model, CIRP Ann. Manuf. Technol. 39 (1990) 201–204, https://doi.org/10.1016/S0007-8506(07)61035-X.
[35] N.A. Ebraheim, F.F. Sabry, Y. Nadim, Internal architecture of the talus: implication for talar fracture, Foot Ankle Int. 20 (1999) 794–796.
[36] X. Cheng, Y. Wang, H. Qu, Y. Jiang, Ossification processes and perichondral ossification groove of Ranvier: a morphological study in developing human calcaneus and talus, Foot Ankle Int. 16 (1995) 7–10, https://doi.org/10.1177/107110079501600102.
[37] H. Fritsch, O. Schmitt, R. Eggers, The ossification centre of the talus, Ann. Anat. 178 (1996) 455–459, https://doi.org/10.1016/S0940-9602(96)80140-3.
[38] C.A. Lill, A.K. Fluegel, E. Schneider, Effect of ovariectomy, malnutrition and glucocorticoid application on bone properties in sheep: a pilot study, Osteoporos. Int. 13 (2002) 480–486, https://doi.org/10.1007/s001980200058.
[39] E. Mittra, C. Rubin, Y.-X. Qin, Interrelationship of trabecular mechanical and microstructural properties in sheep trabecular bone, J. Biomech. 38 (2005) 1229–1237, https://doi.org/10.1016/j.jbiomech.2004.06.007.
[40] S. Schorlemmer, C. Gohl, S. Iwabu, A. Ignatius, L. Claes, P. Augat, Glucocorticoid treatment of ovariectomized sheep affects mineral density, structure, and mechanical properties of cancellous bone, J. Bone Miner. Res. 18 (2003) 2010–2015, https://doi.org/10.1359/jbmr.2003.18.11.2010.
[41] Z. Wu, W. Lei, Y. Hu, H. Wang, S. Wan, Z. Ma, H. Sang, S. Fu, Y. Han, Effect of ovariectomy on BMD, micro-architecture and biomechanics of cortical and cancellous bones in a sheep model, Med. Eng. Phys. 30 (2008) 1112–1118, https://doi.org/10.1016/j.medengphy.2008.01.007.
[42] M. Doube, M.M. Kłosowski, I. Arganda-Carreras, F.P. Cordelières, R.P. Dougherty, J.S. Jackson, B. Schmid, J.R. Hutchinson, S.J. Shefelbine, BoneJ: free and extensible bone image analysis in ImageJ, Bone 47 (2010) 1076–1079, https://doi.org/10.1016/j.bone.2010.08.023.
[43] M.M. Barak, M. Patel, Studying trabecular bone tissue structure-function relationship using 3D printing, Am. J. Phys. Anthropol. 168 (2019) 12.
[44] L. Fiorenza, R. Yong, S. Ranjitkar, T. Hughes, M. Quayle, P.G. McMenamin, J. Kaidonis, G.C. Townsend, J.W. Adams, Technical note: the use of 3D printing in dental anthropology collections, Am. J. Phys. Anthropol. 167 (2018) 400–406, https://doi.org/10.1002/ajpa.23640.
[45] D.P. Fyhrie, M.B. Schaffler, Failure mechanisms in human vertebral cancellous bone, Bone 15 (1994) 105–109, https://doi.org/10.1016/8756-3282(94)90900-8.
[46] M. Hakamada, Y. Asao, T. Kuromura, Y. Chen, H. Kusuda, M. Mabuchi, Density dependence of the compressive properties of porous copper over a wide density range, Acta Mater. 55 (2007) 2291–2299, https://doi.org/10.1016/j.actamat.2006.11.024.
[47] R Core Team, R: A Language and Environment for Statistical Computing, R Foundation for Statistical Computing, Vienna, Austria, 2015https://www.R-project.org.
[48] B. Van Rietbergen, A. Odgaard, J. Kabel, R. Huiskes, Direct mechanics assessment of elastic symmetries and properties of trabecular bone architecture, J. Biomech. 29 (1996) 1653–1657.
[49] G. Bevill, F. Farhamand, T.M. Keaveny, Heterogeneity of yield strain in low-density versus high-density human trabecular bone, J. Biomech. 42 (2009) 2165–2170, https://doi.org/10.1016/j.jbiomech.2009.05.023.
[50] C. Ohman, M. Baleani, E. Perilli, E. Dall'Ara, S. Tassani, F. Baruffaldi, M. Viceconti, Mechanical testing of cancellous bone from the femoral head: experimental errors due to off-axis measurements, J. Biomech. 40 (2007) 2426–2433, https://doi.org/10.1016/j.jbiomech.2006.11.020.
[51] K.L. Troy, M.D. Grabiner, Off-axis loads cause failure of the distal radius at lower magnitudes than axial loads: a finite element analysis, J. Biomech. 40 (2007) 1670–1675, https://doi.org/10.1016/j.jbiomech.2007.01.018.
[52] C.H. Turner, S.C. Cowin, Errors induced by off-axis measurement of the elastic properties of bone, J. Biomech. Eng. 110 (1988) 213–215.
[53] K. Birnbaum, R. Sindelar, J.R. Gaertner, D.C. Wirtz, Material properties of trabecular bone structures, Surg. Radiol. Anat. 23 (2001) 399–407.
[54] W.C. Chang, T.M. Christensen, T.P. Pinilla, T.M. Keaveny, Uniaxial yield strains for bovine trabecular bone are isotropic and asymmetric, J. Orthop. Res. 17 (1999) 582–585, https://doi.org/10.1002/jor.1100170418.
[55] F. Linde, B. Pongsoipetch, L.H. Frich, I. Hvid, Three-axial strain controlled testing applied to bone specimens from the proximal tibial epiphysis, J. Biomech. 23 (1990) 1167–1172.
[56] C.F. Njeh, R. Hodgskinson, J.D. Currey, C.M. Langton, Orthogonal relationships between ultrasonic velocity and material properties of bovine cancellous bone, Med. Eng. Phys. 18 (1996) 373–381.
[57] F. Cavani, M. Fini, F. de Terlizzi, M. Cadossi, L. Ciminelli, S. Ortolani, R. Cherubini, D. De Aloysio, G. Giavaresi, R. Cadossi, V. Canè, Effect of trabecular orientation on mechanical resistance and ultrasound propagation in specimens of equine vertebrae, Ultrasound Med. Biol. 29 (2003) 1777–1785.
[58] A. Hosokawa, Numerical investigation of ultrasound refraction caused by oblique orientation of trabecular network in cancellous bone, IEEE Trans. Ultrason. Ferroelectr. Freq. Control 58 (2011) 1389–1396, https://doi.org/10.1109/TUFFC.2011.1958.
[59] P.H. Nicholson, R. Müller, G. Lowet, X.G. Cheng, T. Hildebrand, P. Rüegsegger, G. van der Perre, J. Dequeker, S. Boonen, Do quantitative ultrasound measurements reflect structure independently of density in human vertebral cancellous bone? Bone 23 (1998) 425–431.
[60] P.H. Nicholson, M.J. Haddaway, M.W. Davie, The dependence of ultrasonic properties on orientation in human vertebral bone, Phys. Med. Biol. 39 (1994) 1013–1024.
[61] P. Augat, T. Link, T.F. Lang, J.C. Lin, S. Majumdar, H.K. Genant, Anisotropy of the elastic modulus of trabecular bone specimens from different anatomical locations, Med. Eng. Phys. 20 (1998) 124–131.
[62] S. Majumdar, M. Kothari, P. Augat, D.C. Newitt, T.M. Link, J.C. Lin, T. Lang, Y. Lu, H.K. Genant, High-resolution magnetic resonance imaging: three-dimensional trabecular bone architecture and biomechanical properties, Bone 22 (1998) 445–454.
[63] R.W. Goulet, S.A. Goldstein, M.J. Ciarelli, J.L. Kuhn, M.B. Brown, L.A. Feldkamp, The relationship between the structural and orthogonal compressive properties of trabecular bone, J. Biomech. 27 (1994) 375–389, https://doi.org/10.1016/0021-9290(94)90014-0.
[64] J.W. Vahey, J.L. Lewis, R. Vanderby Jr., Elastic moduli, yield stress, and ultimate stress of cancellous bone in the canine proximal femur, J. Biomech. 20 (1987) 29–33.
[65] M. Martens, R. Van Audekercke, P. Delport, P. De Meester, J.C. Mulier, The mechanical characteristics of cancellous bone at the upper femoral region, J. Biomech. 16 (1983) 971–983, https://doi.org/10.1016/0021-9290(83)90098-2.
[66] P.R. Townsend, P. Raux, R.M. Rose, R.E. Miegel, E.L. Radin, The distribution and anisotropy of the stiffness of cancellous bone in the human patella, J. Biomech. 8 (1975) 363–367.
[67] M.J. Ciarelli, S.A. Goldstein, J.L. Kuhn, D.D. Cody, M.B. Brown, Evaluation of orthogonal mechanical properties and density of human trabecular bone from the major metaphyseal regions with materials testing and computed tomography, J. Orthop. Res. 9 (1991) 674–682, https://doi.org/10.1002/jor.1100090507.
[68] J.L. Williams, J.L. Lewis, Properties and an anisotropic model of cancellous bone from the proximal tibial epiphysis, J. Biomech. Eng. 104 (1982) 50–56.
[69] T.D. Brown, A.B. Ferguson, Mechanical property distributions in the cancellous bone of the human proximal femur, Acta Orthop. Scand. 51 (1980) 429–437.
[70] J.L. Stone, G.S. Beaupre, W.C. Hayes, Multiaxial strength characteristics of trabecular bone, J. Biomech. 16 (1983) 743–752.
[71] L. Rincón-Kohli, P.K. Zysset, Multi-axial mechanical properties of human trabecular bone, Biomech. Model. Mechanobiol. 8 (2009) 195–208, https://doi.org/10.1007/s10237-008-0128-z.
[72] G.F. Evans, A.I. King, Regional differences in some physical properties of human spongy bone, Biomechanical Studies of the Musculo-skeletal System, Charles C Thomas, Springfield IL, USA, 1961, pp. 49–67.
[73] R.M.V. Pidaparti, C.H. Turner, Cancellous bone architecture: advantages of non-orthogonal trabecular alignment under multidirectional joint loading, J. Biomech. 30 (1997) 979–983, https://doi.org/10.1016/S0021-9290(97)00052-3.
[74] J.C. Behrens, P.S. Walker, H. Shoji, Variations in strength and structure of cancellous one at the knee, J. Biomech. 7 (1974) 201–207, https://doi.org/10.1016/0021-9290(74)90010-4.
[75] M. Matsuura, F. Eckstein, E.-M. Lochmüller, P.K. Zysset, The role of fabric in the quasi-static compressive mechanical properties of human trabecular bone from various anatomical locations, Biomech. Model. Mechanobiol. 7 (2008) 27–42.
[76] P.M. de Bakker, S.L. Manske, V. Ebacher, T.R. Oxland, P.A. Cripton, P. Guy, During sideways falls proximal femur fractures initiate in the superolateral cortex: evidence from high-speed video of simulated fractures, J. Biomech. 42 (2009) 1917–1925, https://doi.org/10.1016/j.jbiomech.2009.05.001.